SIAM REVIEW
Vol. 54, No. 3, pp. 000–000

Chladni Figures and the Tacoma Bridge: Motivating PDE Eigenvalue Problems via Vibrating Plates*

Martin J. Gander†
Felix Kwok†

Abstract. Teaching linear algebra routines for computing eigenvalues of a matrix can be well motivated to students using interesting examples. We propose in this paper to use vibrating plates for two reasons: first there are interesting applications, from which we chose the Chladni figures representing sand ornaments which form on a vibrating plate, and the Tacoma bridge, one of the most spectacular bridge failures. Second, the partial differential operator that arise from vibrating plates is the biharmonic operator, which one does not encounter often in a first course on numerical partial differential equations, and which is more challenging to discretize than the standard Laplacian seen in most textbooks. In addition, the history of vibrating plates is interesting, and we will show both spectral discretizations leading to small dense matrix eigenvalue problems, and a finite difference discretization, leading to large scale sparse matrix eigenvalue problems. Hence both the QR-algorithm and Lanczos can be well illustrated.

Key words. Chladni figures, Ritz method, dense and sparse eigenvalue problems, biharmonic operator discretization

AMS subject classifications. 65-01, 65N30, 65N06, 65N25

DOI. 10.1137/10081931X

1. Introduction.

In 1787, the musician and physicist Ernst Florence Friedrich Chladni from Leipzig made an interesting discovery [7]: he noticed that when he tried to excite a metal plate with the bow of his violin, he could make sounds of different pitch, depending on where he touched the plate with the bow. The plate itself was fixed only in the center, and when there was some dust or sand on the plate, for each pitch a beautiful pattern appeared, see Figure 1.1. These figures, now called Chladni figures after their inventor, attracted great attention among scientists and laymen alike, because of their intriguing beauty, and their calculation proved to be too hard for more than a century. The first mathematical model for the deformation of an elastic plate under an external force was formulated by Sophie Germain in a series of unpublished papers (1811/13/15); a summary of this work appeared in print a few years later [11, 12]. Lagrange and Poisson then added corrections and improvements

*Received by the editors December 28, 2010; accepted for publication (in revised form) September 19, 2011; published electronically August 7, 2012.
http://www.siam.org/journals/sirev/54-3/81931.html
†Section de Mathématiques, Université de Genève, CP 64, 1211 Genève (Martin.Gander@unige.ch, Felix.Kwok@.unige.ch).

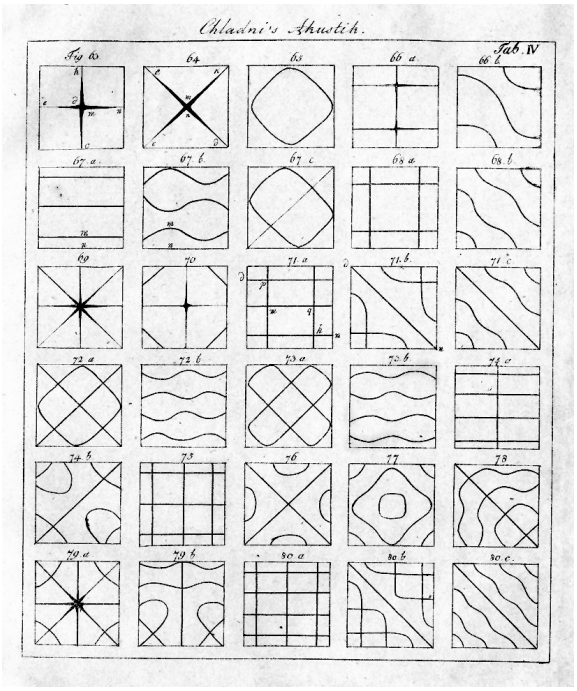

Fig. 1.1 *Drawings of the beautiful figures Chladni obtained when exciting an iron plate with some sand on it, using his violin bow* [7].

to the mathematical model, but the definitive breakthrough was achieved by Kirchhoff in [17], who showed that Chladni figures on a square plate correspond to eigenpairs (eigenvalues and corresponding eigenfunctions) of the biharmonic operator with free boundary conditions. Kirchhoff also managed to solve the problem of Chladni figures on a circular plate, where the many symmetries greatly simplify the problem and solutions. At the turn of the twentieth century, the great expert on the theory of sound, John William Strutt, later Baron Rayleigh, summarized the situation in his monumental treatise [28]: "The Problem of a rectangular plate, whose edges are free, is one of great difficulty, and has for the most part resisted attack". It was only the spectacular invention of Walther Ritz [25], conscious of his imminent death from consumption, which led to the first accurate computation of Chladni figures on square plates in 1909. For more details on the historical development, see [10].

Vibrating plates are very important in many applications. Ritz's method was used right after its invention by Timoshenko for the simulation of beams and plates [29], by Bubnov in the design of submarines [6], and led to the seminal paper of Galerkin [9], also on the simulation of rods and plates. While Galerkin himself calls the method in his paper the Ritz method, after his inventor, it is nowadays better known as the Galerkin method. We will adopt here the historically more correct name Ritz–Galerkin method.

One of the most spectacular examples in engineering of the failure of a structure due to vibrations is the collapse of the Tacoma Narrows bridge in 1940:

> At the time it opened for traffic in 1940, the Tacoma Narrows Bridge was the third longest suspension bridge in the world. It was promptly nick-

> named "Galloping Gertie," due to its behavior in wind. Not only did the deck sway sideways, but vertical undulations also appeared in quite moderate winds. Drivers of cars reported that vehicles ahead of them would completely disappear and reappear from view several times as they crossed the bridge. Attempts were made to stabilize the structure with cables and hydraulic buffers, but they were unsuccessful. On November 7, 1940, only four months after it opened, the Tacoma Narrows Bridge collapsed in a wind of 42 mph — even though the structure was designed to withstand winds of up to 120 mph. [1]

The motion of the Tacoma bridge, which led to its collapse, can be seen in a spectacular movie available on the web[1]. From the movie, we observe that the shape of the center span of the bridge bears a strong resemblance to a thin plate vibrating in one of its eigenmodes; this is also observed in the Ibáñez suspension bridge in Puerto Aysén, Chile, where the bridge motion excited by an earthquake again resembles qualitatively an eigenmode of the thin plate, albeit a different one[2]. If we are interested in approximating the shape of the vibrating bridge span, a very simplified model would be to treat it as a thin vibrating plate and consider the eigenmodes of the biharmonic operator acting on it. This model clearly ignores many structural features of the suspension bridge; in particular, it cannot explain how the bridge was excited in the first place. While many physics textbooks treat this as a classical example of forced resonance, this explanation has been shown to be incorrect in [4]; in fact, a simple physical experiment using a fan and a cardboard box clearly demonstrates that oscillations can be started without periodic forcing [26]. In addition, there is much controversy on whether a linear model can give rise to such large sustained oscillations, or whether a nonlinear one that considers cables and other structures is needed, see [20, 21]. Nonetheless, the vibrating plate model's simplicity and its ability to qualitatively approximate the observed shapes of the vibrating bridges makes it particularly well suited for capturing the student's attention in the context of an introduction to PDE eigenvalue problems.

2. Mathematical Model of Vibrations.

2.1. Equations of Motion. Suppose we have a thin elastic plate $\Omega \subset \mathbb{R}^2$ with unit mass density everywhere (i.e., $\rho(x, y) \equiv \rho = 1$). Intuitively, we say that the plate is vibrating when, after having been set in motion by an initial displacement or external force, the plate continues to bend and oscillate for a very long time without further excitation. One can imagine that the plate would continue to vibrate forever if there are no friction or other damping forces to slow the vibration down. In this case, the only forces that cause the plate to oscillate come from the strain (or bending) energy that has been stored in the plate itself. In particular, the force acting on a given point on the plate depends only on the local shape of the plate. Thus, if we let $z = z(x, y, t)$ be the vertical position of the plate at point (x, y) at time t, then the vertical force acting on this point can be written as

$$F(x, y, t) = -\mathcal{L}z,$$

[1] http://www.youtube.com/watch?v=3mclp9QmCGs
[2] http://www.youtube.com/watch?v=t9kR9T9wZsM

where $\mathcal{L}$ is a *spatial* differential operator acting on z. Since there are no other forces, Newton's law of motion says that

$$\frac{\partial^2 z}{\partial t^2} = -\mathcal{L}z. \tag{2.1}$$

We now show how to derive the operator $\mathcal{L}$. Sophie Germain argued on physical grounds that the strain energy for a small plate element must be proportional to the square of its curvature; Kirchhoff then refined the model and determined that the energy stored in a bent plate with shape $u(x, y)$ is given by

$$J[u(x,y)] := \frac{1}{2}\iint_\Omega \Big(\Big[\frac{\partial^2 u}{\partial x^2} + \frac{\partial^2 u}{\partial y^2}\Big]^2 - 2(1-\mu)\Big[\frac{\partial^2 u}{\partial x^2}\frac{\partial^2 u}{\partial y^2} - \Big(\frac{\partial^2 u}{\partial x \partial y}\Big)^2\Big]\Big)\, dx\, dy, \tag{2.2}$$

where $\mu \in (0, 1)$ is the material constant (which Ritz took to be 0.225 in order to match Chladni's results). Now suppose that we want to deform the plate slightly to obtain a different shape $u(x, y) + \varepsilon v(x, y)$. To do so, we need to put in extra energy to overcome the force $-\mathcal{L}u$ along the distance εv; this extra energy will then be stored in the strain energy of the plate. Thus, we see that

$$J[u + \varepsilon v] = J[u] + \varepsilon \iint_\Omega (\mathcal{L}u)v\, dx\, dy + O(\varepsilon^2). \tag{2.3}$$

If we rearrange (2.3) and let ε tend to zero, we get

$$\iint_\Omega (\mathcal{L}u)v\, dx\, dy = \lim_{\varepsilon\to 0} \frac{J[u+\varepsilon v] - J[u]}{\varepsilon} = \frac{dJ[u+\varepsilon v]}{d\varepsilon}\Big|_{\varepsilon=0}, \tag{2.4}$$

and hence

$$\begin{aligned}\iint_\Omega (\mathcal{L}u)v\, dx\, dy = \iint_\Omega \Big(&\Big[\frac{\partial^2 u}{\partial x^2} + \frac{\partial^2 u}{\partial y^2}\Big]\Big[\frac{\partial^2 v}{\partial x^2} + \frac{\partial^2 v}{\partial y^2}\Big] \\ &- (1-\mu)\Big[\frac{\partial^2 u}{\partial x^2}\frac{\partial^2 v}{\partial y^2} + \frac{\partial^2 u}{\partial y^2}\frac{\partial^2 v}{\partial x^2} - 2\frac{\partial^2 u}{\partial x \partial y}\frac{\partial^2 v}{\partial x \partial y}\Big]\Big)\, dx\, dy.\end{aligned} \tag{2.5}$$

Thus, we have described the force function $\mathcal{L}u$ by how it acts when integrated with an *arbitrary* function v; this is known as the *weak* or *variational* form of the operator. We can also derive the *strong* form of the operator if we integrate by parts twice to remove all derivatives of v (cf. section 2.3).

2.2. An Eigenvalue Problem. In general, a vibrating motion of a plate will consist of a superposition of many modes, each vibrating at a different frequency. Thus, in order to solve (2.1) for $z(x, y, t)$, we will first look for *separable* solutions, i.e., solutions of the form

$$z(x, y, t) = u(x, y) \cdot T(t).$$

These solutions are also called *standing waves*, because only the amplitude, and not the shape of the wave, changes over time. Substituting into (2.1) gives

$$u(x, y)T''(t) = -(\mathcal{L}u)(x, y)T(t).$$

Assuming $T(t) \neq 0$ and $u(x, y) \neq 0$, we can rearrange the above equation to get

$$-\frac{T''(t)}{T(t)} = \frac{\mathcal{L}u(x,y)}{u(x,y)} = \lambda. \tag{2.6}$$

Here λ must be a constant, since the left-hand side is independent of (x, y) and the right-hand side is independent of t. Thus, $T(t)$ must satisfy the *ordinary* differential equation

$$T''(t) + \lambda T(t) = 0.$$

Since the energy of the system must be bounded, we must have $T(t)$ bounded over all time. Thus, λ must be non-negative, so we can write $\lambda = \omega^2$, with

$$T(t) = A\cos\omega t + B\sin\omega t.$$

As for $u(x, y)$, (2.6) gives $\mathcal{L}u = \lambda u$, or, when integrated with an arbitrary v,

$$\iint_\Omega (\mathcal{L}u)v\,dx\,dy = \lambda \iint_\Omega uv\,dx\,dy, \tag{2.7}$$

where the left-hand side is given by (2.5). This is the variational form of an *eigenvalue problem*, for which we must find a non-zero *eigenfunction* $u(x, y)$.

2.3. Strong Form. We will now derive the strong form of the problem (2.7). We will start by rewriting (2.5) using the subscript notation for partial derivatives:

$$\iint_\Omega (\mathcal{L}u)v\,dx\,dy = \iint_\Omega \left[u_{xx}v_{xx} + u_{yy}v_{yy} + \mu(u_{yy}v_{xx} + u_{xx}v_{yy}) + 2(1-\mu)u_{xy}v_{xy}\right] dx\,dy. \tag{2.8}$$

Assuming that the eigenfunction u is sufficiently differentiable and $\partial\Omega$ is sufficiently smooth, we can integrate each term by parts in order to remove the derivatives on v. We can derive the appropriate integration formulas using the divergence theorem

$$\iint_\Omega \nabla\cdot\mathbf{F}\,dx\,dy = \int_{\partial\Omega} \mathbf{F}\cdot\mathbf{n}\,ds,$$

where $\mathbf{F}$ is a vector field and $\mathbf{n} = (n_x, n_y)$ is the unit outward normal vector. If we substitute $\mathbf{F} = (fg, 0)$ and $\mathbf{F} = (0, fg)$ respectively for scalar functions f and g, then we get

$$\iint_\Omega f g_x\,dx\,dy = \int_{\partial\Omega} f g\, n_x\,ds - \iint_\Omega f_x g\,dx\,dy, \tag{2.9}$$

$$\iint_\Omega f g_y\,dx\,dy = \int_{\partial\Omega} f g\, n_y\,ds - \iint_\Omega f_y g\,dx\,dy. \tag{2.10}$$

We can now integrate each term on the right-hand side of (2.8):

$$\iint_\Omega u_{xx}v_{xx}\,dx\,dy = \int_{\partial\Omega} u_{xx}v_x n_x\,ds - \int_{\partial\Omega} u_{xxx}v\,n_x\,ds + \iint_\Omega u_{xxxx}v\,dx\,dy \tag{2.11}$$

$$\iint_\Omega u_{yy}v_{yy}\,dx\,dy = \int_{\partial\Omega} u_{yy}v_y n_y\,ds - \int_{\partial\Omega} u_{yyy}v\,n_y\,ds + \iint_\Omega u_{yyyy}v\,dx\,dy \tag{2.12}$$

$$\iint_\Omega u_{yy}v_{xx}\,dx\,dy = \int_{\partial\Omega} u_{yy}v_x n_x\,ds - \int_{\partial\Omega} u_{xyy}v\,n_x\,ds + \iint_\Omega u_{xxyy}v\,dx\,dy \tag{2.13}$$

$$\iint_\Omega u_{xx}v_{yy}\,dx\,dy = \int_{\partial\Omega} u_{xx}v_y n_y\,ds - \int_{\partial\Omega} u_{xxy}v\,n_y\,ds + \iint_\Omega u_{xxyy}v\,dx\,dy \tag{2.14}$$

$$\iint_\Omega u_{xy}v_{xy}\,dx\,dy = \int_{\partial\Omega} u_{xy}v_x n_y\,ds - \int_{\partial\Omega} u_{xyy}v\,n_x\,ds + \iint_\Omega u_{xxyy}v\,dx\,dy. \tag{2.15}$$

In the case of a rectangular plate, i.e., for $\Omega = (-L,L)\times(-H,H)$, (2.15) can be further transformed as follows. The boundary integral

$$\int_{\partial\Omega} u_{xy}v_x n_y\,ds$$

vanishes along the edges $x = \pm L$ since $n_y = 0$ there. In addition, n_y is constant along each of the remaining edges. Thus, the integral can be rewritten as

$$\begin{aligned}\int_{\partial\Omega} u_{xy}v_x n_y\,ds &= \int_{-L}^{L} u_{xy}(x,H)v_x(x,H)\,dx - \int_{-L}^{L} u_{xy}(x,-H)v_x(x,-H)\,dx\\ &= -\int_{\partial\Omega} u_{xxy}v\,n_y\,ds + u_{xy}(L,H)v(L,H) - u_{xy}(-L,H)v(-L,H)\\ &\quad - u_{xy}(L,-H)v(L,-H) + u_{xy}(-L,-H)v(-L,-H).\end{aligned} \tag{2.16}$$

Substituting (2.11)–(2.14) and (2.16) into (2.7) gives

$$\begin{aligned}0 &= \iint_\Omega (\mathcal{L}u - \lambda u)v\,dx\,dy\\ &= \iint_\Omega (u_{xxxx} + 2u_{xxyy} + u_{yyyy} - \lambda u)v\,dx\,dy\\ &\quad + \int_{\partial\Omega}\big[u_{xx} + \mu u_{yy}\big]\,v_x n_x\,ds - \int_{\partial\Omega}\big[u_{xxx} + (2-\mu)u_{xyy}\big]v\,n_x\,ds\\ &\quad + \int_{\partial\Omega}\big[\mu u_{xx} + u_{yy}\big]\,v_y n_y\,ds - \int_{\partial\Omega}\big[u_{yyy} + (2-\mu)u_{xxy}\big]v\,n_y\,ds\\ &\quad + 2(1-\mu)\big[u_{xy}(L,H)v(L,H) - u_{xy}(-L,H)v(-L,H)\\ &\qquad - u_{xy}(L,-H)v(L,-H) + u_{xy}(-L,-H)v(-L,-H)\big].\end{aligned} \tag{2.17}$$

We see that the right-hand side above contains four types of terms:

- Interior terms (those inside the double integral),
- Terms along the edges $x = \pm L$ (where $n_y = 0$),
- Terms along the edges $y = \pm H$ (where $n_x = 0$),
- Corner terms $(x,y) = (\pm L, \pm H)$.

By picking the appropriate test functions v, for example from all functions that have square integrable derivatives up to second order, we obtain the PDE and boundary conditions for the *strong form* of the eigenvalue problem: find a nontrivial function u and a corresponding value of λ that satisfy

- Interior:

$$u_{xxxx} + 2u_{xxyy} + u_{yyyy} = \lambda u, \qquad (x,y)\in\Omega, \tag{2.18}$$

- Edges:

$$u_{xx} + \mu u_{yy} = 0, \qquad u_{xxx} + (2-\mu)u_{xyy} = 0, \qquad x = \pm L,\ y\in(-H,H), \tag{2.19}$$

$$u_{yy} + \mu u_{xx} = 0, \qquad u_{yyy} + (2-\mu)u_{xxy} = 0, \qquad y = \pm H,\ x\in(-L,L), \tag{2.20}$$

- Corners:

$$u_{xy} = 0, \qquad (x, y) = (\pm L, \pm H). \tag{2.21}$$

Historically, the interior equation (2.18) was already known by Sophie Germain, but her edge conditions were incorrect; this is because her energy functional lacked the μ-dependent cross terms that influence only the boundary but not the interior equations. The correct edge conditions (2.19), (2.20) have been derived in 1850 by Kirchoff [17], but one had to wait another four decades for the appearance of the corner conditions in the work of Lamb [19], in order to have the complete set of boundary conditions for a thin plate whose boundaries are completely free to move.

2.4. Minimax Principle. Another characterization of the eigenvalues of $\mathcal{L}$ is given by the minimax principle [30, 27]. Assume that the eigenvalues are indexed in ascending order of magnitude, i.e., $\lambda_1 \le \lambda_2 \le \cdots$. Then the kth eigenvalue λ_k satisifies

$$\lambda_k = \min_{\dim U = k} \max_{\substack{u \in U \\ u \neq 0}} \frac{\langle u, \mathcal{L}u \rangle}{\langle u, u \rangle}, \tag{2.22}$$

where the inner product $\langle \cdot, \cdot \rangle$ is defined as

$$\langle u, v \rangle := \iint_\Omega uv \, dx \, dy,$$

and U is a subspace of dimension k consisting of functions that have square integrable derivatives up to second order[3]. The quantity being maximized in (2.22) is called the *Rayleigh quotient*, and the outer minimum is taken over all k-dimensional subspaces of trial functions. Note that one does not need to impose the natural or free boundary conditions (2.19), (2.20) and (2.21) in the space U, since they are automatically satisfied by the solution to the min-max problem, see for example [15].

To see why the min-max formulation (2.22) makes sense, suppose we choose U to be spanned by the first k eigenfunctions $u_1, \ldots, u_k$. Then the largest Rayleigh quotient is attained by setting $u = u_k$. On the other hand, assume U to be any other k-dimensional subspace spanned by $\{w_1, \ldots, w_k\}$. Our goal is to pick a $w \in U$ that gives a Rayleigh quotient that is larger than λ_k. Indeed, there is a nontrivial $w = \sum_{i=1}^k \alpha_i w_i \in U$ such that $\langle w, u_j \rangle = 0$ for $j = 1, \ldots, k-1$, since the $(k-1) \times k$ homogeneous linear system

$$\sum_{i=1}^{k} \alpha_i \langle w_i, u_j \rangle = 0, \qquad j = 1, \ldots, k-1$$

has a nontrivial solution $\alpha = (\alpha_1, \ldots, \alpha_k)^T$. Now if we express w in the eigenbasis $\{u_1, u_2, \ldots\}$, we get

$$w = \sum_{i=k}^{\infty} \beta_i u_i,$$

[3]Although the appearance of $\mathcal{L}u$ in the inner product seems to require higher regularity for u, only second derivatives are really needed, since $\langle u, \mathcal{L}u \rangle$ should be interpreted in the weak sense, i.e., in the sense of (2.5).

since the first $k-1$ coefficients are zero due to orthogonality. Thus, we obtain

$$\langle w, \mathcal{L}w\rangle = \sum_{i=k}^{\infty} \beta_i^2 \lambda_i \geq \lambda_k \sum_{i=k}^{\infty} \beta_i^2 = \lambda_k \langle w, w\rangle.$$

Hence, for any k-dimensional subspace U, the maximum Rayleigh quotient is necessarily greater than or equal to λ_k, which proves the minimax principle.

By choosing the k-dimensional subspace U wisely, it is possible to obtain very good approximations of the eigenvalues and eigenfunctions of $\mathcal{L}$. In section 3.1, we will show how Ritz achieved this.

3. Discretization.

3.1. The Idea of Ritz. Walther Ritz presented in [25] what one would probably call a spectral method nowadays for the computation of vibration modes of a plate; indeed, he was the first person to be able to compute these modes. The main idea of Ritz was not to directly tackle the strong form of the eigenvalue problem (2.18), but instead to try to approximate the eigenvalues using the minimax principle (2.22) with a well-chosen finite-dimensional subspace of functions, which leads naturally to a numerical method[4] . As we have seen, any choice of subspace U results in approximate eigenvalues that are overestimations of the exact ones.

We first need to relate $\langle u, \mathcal{L}u\rangle$ to the energy functional $J[u]$ defined in (2.2). By letting $v = u$ in (2.4), we have

$$\iint_\Omega u(\mathcal{L}u)\, dx\, dy = \frac{dJ[(1+\varepsilon)u]}{d\varepsilon}\Big|_{\varepsilon=0}.$$

But from (2.2), we see that

$$J[(1+\varepsilon)u] = (1+\varepsilon)^2 J[u],$$

so that

$$\langle u, \mathcal{L}u\rangle = 2J[u] = \iint_\Omega \Big(\Big[\frac{\partial^2 u}{\partial x^2} + \frac{\partial^2 u}{\partial y^2}\Big]^2 - 2(1-\mu)\Big[\frac{\partial^2 u}{\partial x^2}\frac{\partial^2 u}{\partial y^2} - \Big(\frac{\partial^2 u}{\partial x \partial y}\Big)^2\Big]\Big)\, dx\, dy. \tag{3.1}$$

The full min-max problem (2.22) is too hard to solve, since we need to consider all possible k-dimensional subspaces of an infinite-dimensional function space. To make the problem more tractable, Ritz decided to solve a smaller min-max problem in which the minimum is taken only over k-dimensional subspaces of a well-chosen finite-dimensional function space U_s. He opted for linear combinations of functions of the form

$$w_{mn}(x, y) = u_m(x) u_n(y),$$

where $u_m(x)$ are the eigenfunctions of a free one-dimensional bar,

$$\frac{d^4 u_m}{dx^4} = k_m^4 u_m, \quad \text{with } \frac{d^2 u_m}{dx^2} = 0,\ \frac{d^3 u_m}{dx^3} = 0 \text{ at } x = \{-1, 1\}.$$

[4] In fact, Ritz focused on the first eigenmode and used a Lagrange multiplier for the normalization constraint, see [25] for this concrete formulation, and also [10]. He however noted that higher modes could also be obtained using further orthogonalization constraints.

With his physical insight, Ritz expected these functions to give very good approximations of the exact two-dimensional eigenfunctions, leading to very accurate eigenvalue approximations. The one-dimensional eigenfunctions are known in closed form [28]:

(3.2)
$$u_m(x) = \begin{cases} \dfrac{\cosh k_m \cos k_m x + \cos k_m \cosh k_m x}{\sqrt{\cosh^2 k_m + \cos^2 k_m}}, & \tan k_m + \tanh k_m = 0, \quad m \text{ even}, \\ \dfrac{\sinh k_m \sin k_m x + \sin k_m \sinh k_m x}{\sqrt{\sinh^2 k_m - \sin^2 k_m}}, & \tan k_m - \tanh k_m = 0, \quad m \text{ odd}. \end{cases}$$

By restricting our search to functions of this type, we are in fact solving the smaller min-max problem

$$\hat{\lambda}_k = \min_{\substack{\dim U = k \\ U \subset U_s}} \max_{\substack{u \in U \\ u \neq 0}} \frac{\langle u, \mathcal{L}u \rangle}{\langle u, u \rangle}, \tag{3.3}$$

where U_s consists of functions of the form

$$w_s(x,y) := \sum_{m=0}^{s} \sum_{n=0}^{s} a_{mn} u_m(x) u_n(y).+ \tag{3.4}$$

Again, these functions do not satisfy the free boundary conditions (2.19), (2.20) and (2.21), but they do not need to. Since the w_s are parameterized by the coefficients a_{mn}, (3.3) can be rewritten as

$$\hat{\lambda}_k = \min_{\substack{\dim U = k \\ U \subset \mathbb{R}^N}} \max_{\substack{\mathbf{a} \in U \\ \mathbf{a} \neq 0}} \frac{\mathbf{a}^T \tilde{K} \mathbf{a}}{\mathbf{a}^T \mathbf{a}}, \tag{3.5}$$

where $\mathbf{a} := [a_{00}, a_{01}, a_{10}, \ldots] \in \mathbb{R}^N$, $N = (s+1)^2$, and $\tilde{K}$ is the $N \times N$ matrix

$$\widetilde{K} := \begin{bmatrix} k_{00}^{00} & k_{01}^{00} & k_{10}^{00} & \cdots \\ k_{00}^{01} & k_{01}^{01} & k_{10}^{01} & \cdots \\ k_{00}^{10} & k_{01}^{10} & k_{10}^{10} & \cdots \\ \vdots & \vdots & \vdots & \ddots \end{bmatrix}.$$

The coefficients k_{mn}^{pq} are obtained by inserting w_s into the quadratic form $\langle w_s, \mathcal{L} w_s \rangle = 2J[w_s]$:

$$\begin{aligned} k_{mn}^{pq} := \int_{-1}^{1} \int_{-1}^{1} & \frac{\partial^2 u_m(x)}{\partial x^2} u_n(y) \frac{\partial^2 u_p(x)}{\partial x^2} u_q(y) dx dy + u_m(x) \frac{\partial^2 u_n(y)}{\partial y^2} u_p(x) \frac{\partial^2 u_q(y)}{\partial y^2} dx dy \\ & + 2\mu \frac{\partial^2 u_m(x)}{\partial x^2} u_n(y) \frac{\partial^2 u_q(y)}{\partial y^2} u_p(x) + 2(1-\mu) \frac{\partial u_m(x)}{\partial x} \frac{\partial u_n(y)}{\partial y} \frac{\partial u_p(x)}{\partial x} \frac{\partial u_q(y)}{\partial y} dx dy. \end{aligned}$$

But (3.5) is the minimax characterization of a matrix eigenvalue problem, namely

$$K \mathbf{a} = \hat{\lambda} \mathbf{a}, \tag{3.6}$$

where $K := \frac{1}{2}(\widetilde{K} + \widetilde{K}^T)$ is a symmetric matrix of size $N \times N$. For each eigenvalue $\hat{\lambda}_\ell$, we get an associated eigenvector $\mathbf{a}_\ell = [a_{00}^\ell, a_{01}^\ell, \ldots]$, and thus the corresponding approximate eigenfunction

$$w_s^\ell = \sum_{m=0}^{s} \sum_{n=0}^{s} a_{mn}^\ell u_m(x) u_n(y).$$

Since K is a small dense matrix and we want to compute all (or most of) its eigenvalues, a method such as the QR algorithm would be appropriate for this purpose.

In order to compute concrete examples, it is best to use a symbolic computing program, since the evaluation of the integrals is quite tedious. We start by defining the one-dimensional vibration modes using Maple:

```
k:=m->if type(m,even) then
  fsolve(tan(x)+tanh(x)=0,x=m*Pi/2-Pi/4)
else
  fsolve(tan(x)-tanh(x)=0,x=(m-1/2)*Pi/2)
end if;
u:=(m,x)->if m=0 then
  1/sqrt(2)
elif m=1 then
  sqrt(3/2)*x
elif type(m,even) then
  (cosh(k(m))*cos(k(m)*x)+cos(k(m))*cosh(k(m)*x))/sqrt((cosh(k(m)))^2+(cos(k(m)))^2)
  else
  (sinh(k(m))*sin(k(m)*x)+sin(k(m))*sinh(k(m)*x))/sqrt((sinh(k(m)))^2-(sin(k(m)))^2)
end if;
```

We can now evaluate the various integrals in order to obtain the coefficients k_{mn}^{pq}, which are then stored in the matrix $\widetilde{K}$:

```
with(LinearAlgebra):
N:=6;                        # number of modes in each direction
mu:=0.225;                   # material parameter
Kt := Matrix(1..(N+1)^2,1..(N+1)^2);
i:=0;
for m from 0 to N do
 for n from 0 to N do
   i:=i+1; j:=0;
   for p from 0 to N do
     for q from 0 to N do
       j:=j+1;
       if type(m+p,even) and type(n+q,even) then   #Do not calculate zeros
         Kt[i,j]:=evalf(Int(Int(diff(u(m,x),x,x)*u(n,y)*diff(u(p,x),x,x)*u(q,y),x=-1..1),y=-1..1)
          +Int(Int(diff(u(n,y),y,y)*u(m,x)*diff(u(q,y),y,y)*u(p,x),x=-1..1),y=-1..1)
          +2*mu*Int(Int(diff(u(m,x),x,x)*u(n,y)*diff(u(q,y),y,y)*u(p,x),x=-1..1),y=-1..1)
          +2*(1-mu)*Int(Int(diff(u(m,x),x)*diff(u(n,y),y)*diff(u(p,x),x)*diff(u(q,y),y),x=-1..1),y=-1..1));
       fi;
     od;
   od;
 od;
od;
```

Observe that there is an if-statement inside the quadruple loop that only executes when m and p (resp. n and q) have the same parity (i.e., when they are both even or both odd). This is because all other coefficients must be zero; the proof uses the many orthogonality relations satisfied by the 1D eigenfunctions $u_m(x)$ (cf. [25]). Thus, we can save computing time by omitting the calculation of these zero entries.

We can now compute the eigenvalues and eigenvectors of K, and then construct the approximate eigenfunctions:

```
V,E:=Eigenvectors(Matrix((Kt+Transpose(Kt))/2,shape=symmetric));
for i from 1 to (N+1)^2 do
 j:=0:
 U[i]:=0:
 for m from 0 to N do
   for n from 0 to N do
```

```
      j:=j+1:
      U[i]:=U[i]+E[j,i]*u(m,x)*u(n,y):
    od:
  od:
od:
```

It remains to draw the zero level set of the approximate eigenfunctions we have construced, which is achieved by the Maple commands

```
with(plots):
for i from 4 to (N+1)^2 do
  contourplot(U[i],x=-1..1,y=-1..1,grid=[200,200],contours=[0],axes=boxed,view=[-1..1,-1..1]);
od;
```

This leads to the results shown in Figure 4.1.

3.2. Finite Difference Discretization. A different approach would be to discretize the strong form of the eigenvalue problem (2.18)–(2.21) using finite differences. The fact that the PDE contains the biharmonic operator Δ^2 suggests that we should build the discretization by composing the discrete 5-point Laplacian operator Δ_h with itself; indeed, this will give the correct stencil for nodes away from the boundary, as we will see in (3.9). However, the discretization of the free boundary conditions (2.19)–(2.21), which are necessary in the strong form, is less obvious. Our approach here is to use a finite volume method to deal with these cases systematically.

Let $\Omega = (-1,1) \times (-1,1)$ be the square plate, which we discretize on a uniform $(N+1)\times(N+1)$ grid, including nodes on the boundary. Then the grid points (x_i, y_j), $0 \le i, j \le N$ satisfy

$$x_i = -1 + ih, \qquad y_j = -1 + jh, \qquad h = 2/N.$$

Let $u(x,y)$ be the exact solution of the eigenvalue problem, and $u_{ij} \approx u(x_i, y_j)$ be its finite difference approximation. We first define $w(x,y) = -\Delta u(x,y)$ and its discrete analog

$$w_{ij} = \frac{4u_{ij} - u_{i-1,j} - u_{i+1,j} - u_{i,j-1} - u_{i,j+1}}{h^2}. \tag{3.7}$$

Note that in order to define w_{ij} along an edge, we need values of u_{ij} that fall outside Ω, i.e., for $i, j \in \{-1, N+1\}$. These are called ghost points and are not part of the original problem; they will need to be eliminated using boundary conditions before we solve the discrete eigenvalue problem. Once we have defined $w(x,y)$, the strong form of the PDE now says

$$\Delta^2 u = \lambda u \iff -\Delta w = \lambda u.$$

To obtain a finite volume method, we need to integrate over a control volume V_{ij} around each grid point. Figure 3.1 shows the control volumes for an interior point, an edge point and a corner point. Integrating the strong form of the PDE over V_{ij} gives

$$-\iint_{V_{ij}} \Delta w \, dx\, dy = \lambda \iint_{V_{ij}} u(x,y)\, dx\, dy,$$

to which we can invoke the divergence theorem to get

$$-\int_{\partial V_{ij}} \frac{\partial w}{\partial n}\, ds = \lambda \iint_{V_{ij}} u(x,y)\, dx\, dy.$$

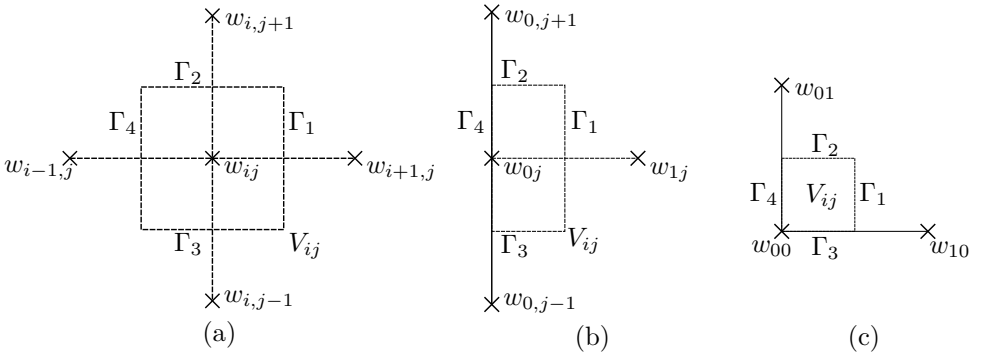

Fig. 3.1 *Control volumes for different types of nodes:* (a) *interior nodes,* (b) *edge nodes,* (c) *corner nodes.*

The integral on the right-hand side is approximated by (cf. Figure 3.1)

$$\iint_{V_{ij}} u(x,y)\,dx\,dy \approx |V_{ij}|u_{ij} = \begin{cases} h^2 u_{ij} & \text{for interior nodes,} \\ \frac{1}{2}h^2 u_{ij} & \text{for edge nodes,} \\ \frac{1}{4}h^2 u_{ij} & \text{for corner nodes.} \end{cases} \tag{3.8}$$

The fluxes $\int \frac{\partial w}{\partial n}\,dx$ on the left-hand side must be approximated differently for the different types of nodes.

3.2.1. Interior Nodes. The flux along each piece of ∂V_{ij} is simply approximated by a finite difference. For example, along Γ_1 shown on Figure 3.1(a), we take

$$\int_{\Gamma_1} \frac{\partial w}{\partial n}\,ds \approx h \cdot \frac{w_{i+1,j} - w_{ij}}{h},$$

which leads to the standard finite difference stencil for w:

$$-\int_{\partial V_{ij}} \frac{\partial w}{\partial n}\,ds \approx 4w_{ij} - w_{i-1,j} - w_{i+1,j} - w_{i,j-1} - w_{i,j+1}. \tag{3.9}$$

Thus, the interior stencil is indeed the discrete Laplacian squared, i.e., we approximate Δ^2 by Δ_h^2.

3.2.2. Edge Nodes. We consider a control volume along the left edge $x = x_0 = -1$, as shown in Figure 3.1(b); the other edges are treated similarly. The fluxes along Γ_1, Γ_2 and Γ_3 are approximated in the same way as for interior nodes, except there is a factor of $1/2$ for the top and bottom contributions, since the length of those edges is only $h/2$. Thus, we get

$$-\int_{\partial V_{0j}} \frac{\partial w}{\partial n}\,ds \approx 2w_{0j} - w_{1j} - \frac{1}{2}w_{0,j-1} - \frac{1}{2}w_{0,j+1} - \int_{\Gamma_4} \frac{\partial w}{\partial n}\,ds. \tag{3.10}$$

To approximate the integral along Γ_4, we must make use of the boundary conditions. We have

$$\int_{\Gamma_4} \frac{\partial w}{\partial n}\,ds = \int_{y_{j-1/2}}^{y_{j+1/2}} \frac{\partial}{\partial x}(u_{xx} + u_{yy})\,dy$$

$$
\begin{aligned}
&= \int_{y_{j-1/2}}^{y_{j+1/2}} \big[\underbrace{u_{xxx} + (2-\mu)u_{xyy}}_{=0} - (1-\mu)u_{xyy}\big]\, dy \\
&= -(1-\mu)\int_{y_{j-1/2}}^{y_{j+1/2}} u_{xyy}\, dy \\
&= -(1-\mu)\big[u_{xy}(x_0, y_{j+1/2}) - u_{xy}(x_0, y_{j-1/2})\big].
\end{aligned}
$$

The mixed derivatives u_{xy} can now be approximated by finite differences, e.g.,

$$
u_{xy}(x_0, y_{j-1/2}) \approx \frac{u_{1,j} - u_{-1,j} - u_{1,j-1} + u_{-1,j-1}}{2h^2}. \tag{3.11}
$$

3.2.3. Corner Nodes. The control volume corresponding to a corner node has two edges in the interior of Ω and two edges along $\partial\Omega$. Thus, for the corner cell in Figure 3.1(c), we have

$$
-\int_{\partial V_{ij}} \frac{\partial w}{\partial n}\, ds \approx w_{00} - \frac{1}{2}w_{10} - \frac{1}{2}w_{01} - \int_{\Gamma_3} \frac{\partial w}{\partial n}\, ds - \int_{\Gamma_4} \frac{\partial w}{\partial n}\, ds. \tag{3.12}
$$

To evaluate the integrals along Γ_3 and Γ_4, we perform the same calculations as for the edge case to obtain, for instance,

$$
\int_{\Gamma_4} \frac{\partial w}{\partial n}\, ds = -(1-\mu)\big[u_{xy}(x_0, y_{1/2}) - u_{xy}(x_0, y_0)\big].
$$

But $u_{xy} = 0$ at the corner; thus, the second term on the right-hand side simply drops, and we in fact have

$$
\int_{\partial V_{ij}} \frac{\partial w}{\partial n}\, ds \approx w_{00} - \frac{1}{2}w_{10} - \frac{1}{2}w_{01} + (1-\mu)u_{xy}(x_0, y_{1/2}) + (1-\mu)u_{xy}(x_{1/2}, y_0),
$$

where the mixed derivatives are discretized as in (3.11).

3.2.4. Ghost Points. As mentioned before, values of u_{ij} that fall outside the physical boundary Ω are simply defined for convenience and must be eliminated before the eigenvalue problem is solved. Fortunately, this can be done easily using the edge boundary conditions

$$
u_{xx} + \mu u_{yy} = 0 \quad \text{for } x = \pm 1, \qquad u_{yy} + \mu u_{xx} = 0 \quad \text{for } y = \pm 1.
$$

Thus, for a ghost point along the left edge $x = -1$, we have

$$
u_{-1,j} = 2(1+\mu)u_{0j} - u_{1j} - \mu u_{0,j-1} - \mu u_{0,j+1}. \tag{3.13}
$$

Similar relations can be derived for other ghost points away from the corner. Near the corner, there will be a coupling between the two ghost points attached to the corner, e.g.

$$
\begin{aligned}
u_{-1,0} + \mu u_{0,-1} &= 2(1+\mu)u_{00} - u_{10} - \mu u_{01}, \\
\mu u_{-1,0} + u_{0,-1} &= 2(1+\mu)u_{00} - \mu u_{10} - u_{01}.
\end{aligned}
$$

Since $\mu \neq 1$, we can solve a 2×2 system to obtain equations for $u_{-1,0}$ and $u_{0,-1}$ that depend only on u_{00}, u_{01} and u_{10}. However, as we will see in the next section, it is unnecessary to do this calculation by hand in an actual MATLAB implementation.

```
0  0  0  0  0  0  0  0  0  0
0  .  g  g  g  g  g  g  .  0
0  g  b  b  b  b  b  b  g  0
0  g  b  x  x  x  x  b  g  0
0  g  b  x  x  x  x  b  g  0
0  g  b  x  x  x  x  b  g  0
0  g  b  x  x  x  x  b  g  0
0  g  b  b  b  b  b  b  g  0
0  .  g  g  g  g  g  g  .  0
0  0  0  0  0  0  0  0  0  0
```

Fig. 3.2 *Position of interior nodes* (`x`)*, boundary nodes* (`b`) *and ghost points* (`g`) *for* `n = 8`.

3.2.5. MATLAB Implementation. MATLAB already contains built-in commands for generating a grid on a square and calculating the 5-point Laplacian with Dirichlet boundary conditions:

```
G = numgrid('S', n+2);  % Generate square grid with n points per side
D = delsq(G);           % Construct 5-point Laplacian for G
```

We could attempt to construct the bilaplacian operator by simply calculating `D*D`, but this would give the wrong discretization near the boundary. Our goal is to construct the correct discrete eigenvalue problem by making only minor modifications to D. In particular, we will construct two operators N and L that are identical to D away from the boundary, such that $\mathbf{w} = L\mathbf{u}$ and the product $N\mathbf{w} = NL\mathbf{u}$ gives the correct stencil everywhere.

First, we must carefully identify the grid points in `G` corresponding to interior, boundary and ghost points. The following commands lead to the labeling in Figure 3.2:

```
% Define boundary and ghost points
bl = G(3:n,3); br = G(3:n,n);   bt = G(3,3:n)'; bb = G(n,3:n)';
gl = G(3:n,2); gr = G(3:n,n+1); gt = G(2,3:n)'; gb = G(n+1,3:n)';
```

We now construct the matrices N and L. By (3.9), the part of N corresponding to interior points coincides with the standard 5-point Laplacian matrix. Thus, by setting `N = D`, only rows corresponding to boundary and ghost points need to be adjusted.

Boundary Point Adjustment. If we define $w_{-1,j} := \int_{\Gamma_4} \frac{\partial w}{\partial n}\, ds$, then (3.10) becomes

$$-\int_{\partial V_{0j}} \frac{\partial w}{\partial n}\, ds \approx 2w_{0j} - w_{1j} - \frac{1}{2}w_{0,j-1} - \frac{1}{2}w_{0,j+1} - w_{-1,j}. \tag{3.14}$$

Thus, when compared with the interior stencil, the coefficients with respect to boundary variables need to be halved, whereas those corresponding to interior or ghost points remain unchanged. For the left boundary, this adjustment can be done simply using

```
N(bl,bl) = N(bl,bl)/2;
```

the other boundaries are adjusted similarly. Note that corner points will be adjusted twice (once for each edge they touch), which is exactly what we want: the stencil

(3.12) can be rewritten as

$$-\int_{\partial V_{ij}} \frac{\partial w}{\partial n}\, ds \approx w_{00} - \frac{1}{2}w_{10} - \frac{1}{2}w_{01} - w_{0,-1} - w_{-1,0}, \tag{3.15}$$

where $w_{0,-1} := \int_{\Gamma_3} \frac{\partial w}{\partial n}\, ds$, $w_{-1,0} := \int_{\Gamma_4} \frac{\partial w}{\partial n}\, ds$. Thus, we need to divide each of the boundary coefficients by 2 and the diagonal by 4, which is equivalent to adjusting for each edge separately.

Defining w at Ghost Points. For interior and boundary points, w is defined by (3.7) as minus the discrete Laplacian of u. In principle, w is not defined at ghost points; however, (3.14) and (3.15) suggest that it would be convenient to define them as fluxes across the physical boundary, which involve mixed derivatives u_{xy} at half points $(x_0, y_{j+1/2})$. In other words, we need to *replace the rows of L* corresponding to ghost points by *stencils for u_{xy}*. Note that the term $u_{xy}(x_0, y_{j+1/2})$ appears in both $w_{-1,j}$ and $w_{-1,j+1}$, which means we only need to calculate its stencil once. The following loop computes the stencil corresponding to $u_{xy}(x_0, y_{j+1/2})$ and updates both rows j and $j+1$ at the same time. (This trick is similar to assembling finite element matrices by looping through the elements instead of the nodes.)

```
for j=gl(1:end-1)',  % left boundary
    L([j,j+1],[j,j+1,j+2*n,j+2*n+1]) = ...
    L([j,j+1],[j,j+1,j+2*n,j+2*n+1]) + (mu-1)/2*[1,-1,-1,1;-1,1,1,-1];
end;
```

Eliminating Ghost Points. If we now form the product `A = N*L`, the stencil would be correct everywhere. However, this system is too large: the eigenvalue problem should only contain points in the physical domain and not ghost points. Thus, we need to eliminate the ghost points using boundary conditions of the type (3.13). Since the rows of A corresponding to ghost points are spurious anyway, we can replace them by equations of the type (3.13):

```
A(gl,:) = 0;  % left ghost points
for i=gl',
    A(i,[i+n,i,i+n-1,i+n+1,i+2*n]) = [2*(1+mu), -1, -mu, -mu, -1];
end;
```

Once all the boundary conditions are in place, we are ready to eliminate the ghost points to obtain a system that contains only points in the physical domain. This is done by taking a Schur complement with respect to the ghost points:

```
phys = G(3:n,3:n); phys = phys(:); % put all physical nodes in a vector
ghost = [gl; gr; gt; gb];
A0 = A(phys,phys) - A(phys,ghost)/A(ghost,ghost)*A(ghost,phys);
```

It remains now to solve the generalized eigenvalue problem

$$A_0 u = \lambda B u,$$

where B is a diagonal matrix with h^2 for interior points, $h^2/2$ for edge points and $h^2/4$ for corner points (cf. (3.8)). The full program is shown in Appendix A. Note that A_0 is a very large but sparse matrix, of size $(N+1)^2 \times (N+1)^2$ but with each row containing at most 13 non-zero entries. In addition, we are only interested in the first few eigenmodes (the lowest 50 or so), since the higher modes are very

poor approximations of the continuous eigenfunctions. This means one should use a method such as Lanczos to compute these eigenvalues.

4. Numerical Results.

4.1. Chladni Figures. If we compare the two sets of Chladni figures obtained by the spectral and finite difference methods, we notice the following differences:

- For simple modes (eigenvalues with multiplicity 1, which correspond to $m+n$ even), the figures are identical except when both m and n are large. This

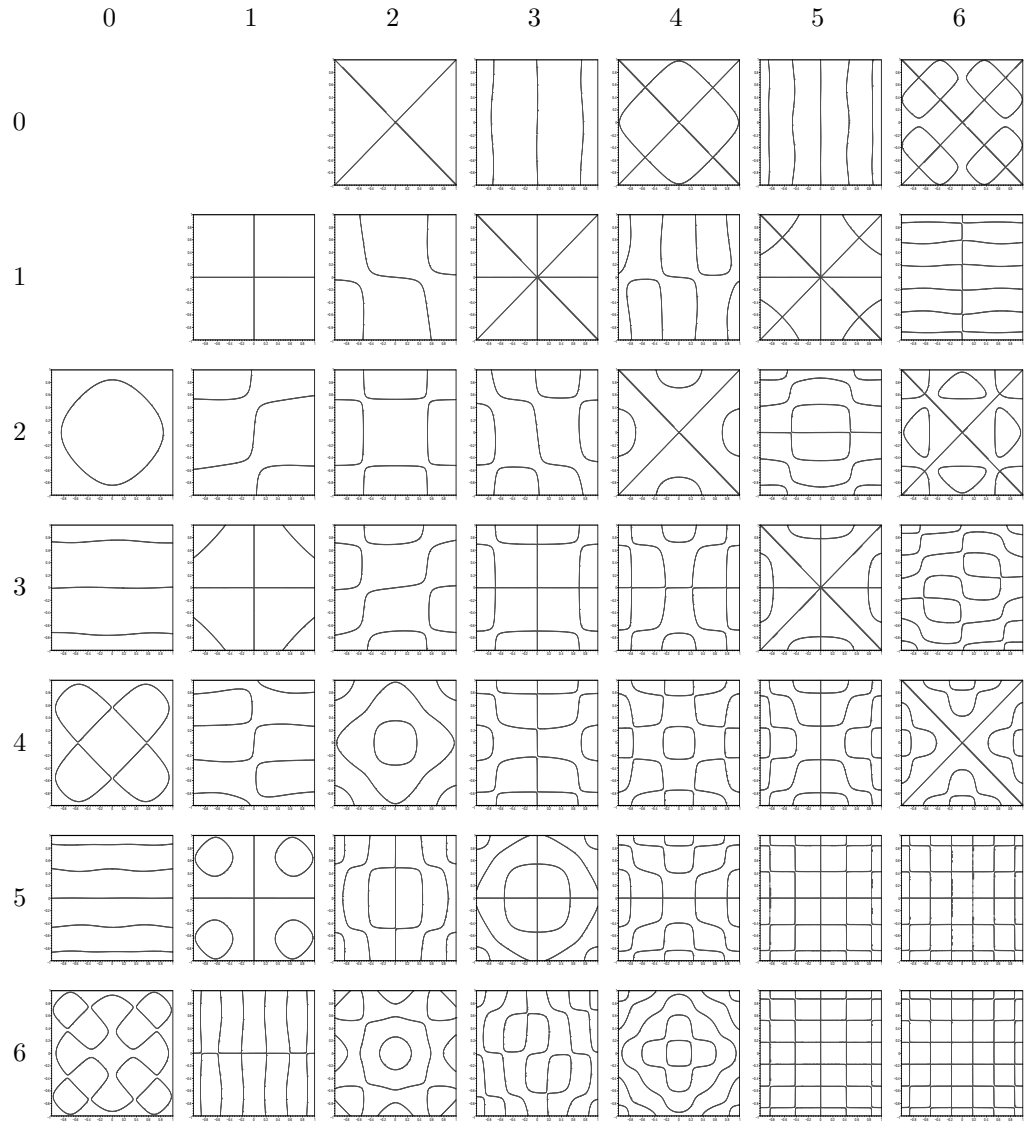

Fig. 4.1 *Chladni figures computed using the spectral method invented by Ritz, arranged according to the leading mode* w_{mn}, $m, n \leq 6$

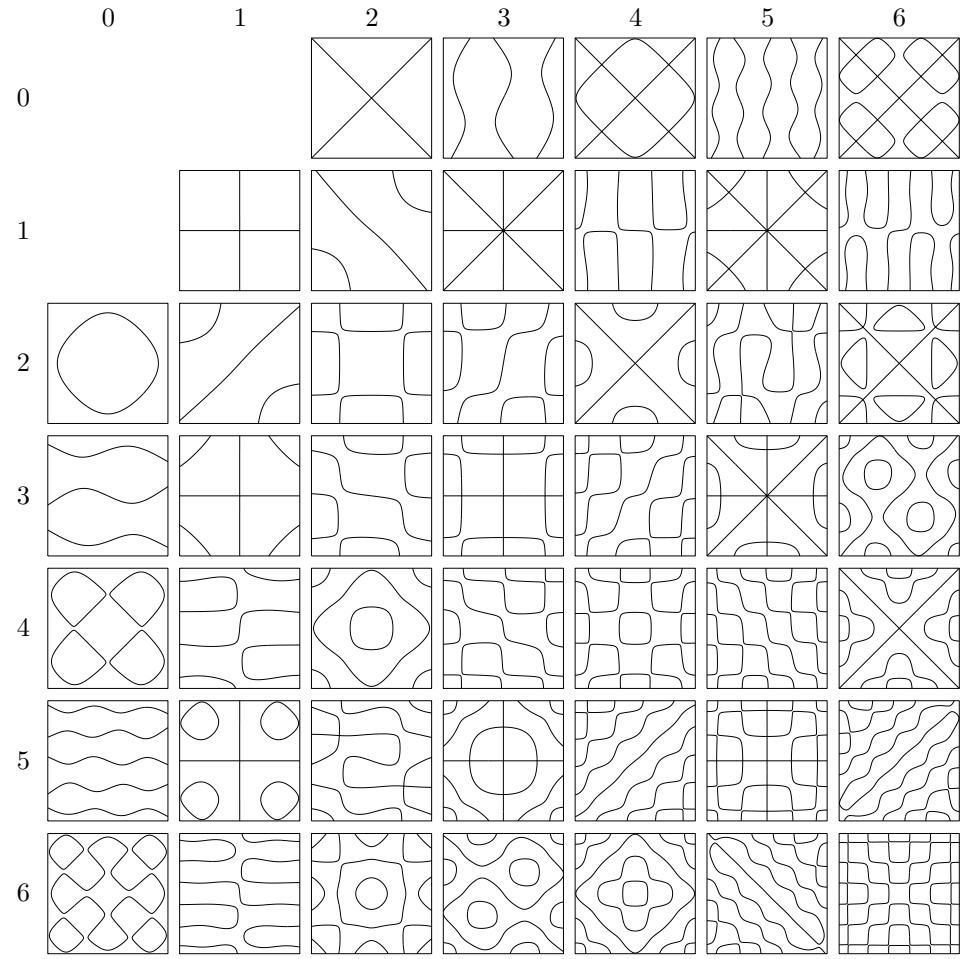

Fig. 4.2 *Chladni figures computed using the finite difference method with* 100 *grid points per direction, arranged in the same way as Figure* 4.1.

confirms that the two approaches really do solve the same eigenvalue problem, since the resulting eigenvectors are the same.

- For double modes (eigenvalues with multiplicity 2, which occur when $m + n$ is odd), the two sets of figures have a similar shape, but they could be mirror images and/or slight perturbations of one another. This happens because the choice of orthogonal basis for the corresponding eigenspace is not unique.
- For higher modes ($m, n \geq 5$), the figures generated by the spectral method begin to lose detail, e.g., nodal lines begin to intersect when they should curve and avoid each other. This is because we only used a small number of spectral basis functions $0 \leq m, n \leq 6$. By increasing the number of basis functions, we recover the same Chladni figures as the finite difference case, which have been generated with 100 grid points per direction (see Figure 4.3).

4.2. Comparison with Chladni and Ritz. We now compare the eigenvalues we computed with the historical results of Chladni and Ritz. Table 4.1 shows the first 15 eigenvalues computed by the two methods. Observe that the spectral eigenvalues form

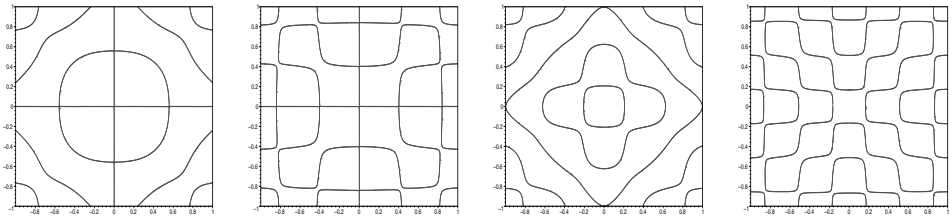

Fig. 4.3 *Chladni figures obtained by the spectral method using 10 basis functions per direction (*$0 \leq m, n \leq 9$*).*

Table 4.1 *First* 15 *eigenvalues obtained using the spectral and finite difference discretizations, together with their position in Figures* 4.1 *and* 4.2*; an asterisk means the row corresponds to a double eigenvalue. For the spectral method,* N *is the number of basis functions in each direction in the Galerkin approximation; for finite differences,* N *is the number of grid points in each direction. The relative gap between the two methods (with the largest* N*) are shown.*

	Spectral				Finite Difference			Gap
N	7	8	9	10	100	200	400	
(1,1)	12.5	12.5	12.5	12.5	12.4	12.5	12.5	0.08%
(0,2)	26.2	26.1	26.1	26.1	26.0	26.0	26.0	0.46%
(2,0)	35.8	35.8	35.8	35.8	35.6	35.6	35.6	0.36%
(2,1)*	81.3	81.2	81.2	81.2	80.8	80.9	80.9	0.36%
(3,0)*	236.7	236.4	236.4	236.3	234.9	235.3	235.4	0.39%
(2,2)	271.0	270.2	270.2	270.0	269.0	269.3	269.3	0.24%
(1,3)	322.5	322.5	322.4	322.4	320.1	320.5	320.7	0.53%
(3,1)	377.8	377.8	377.2	377.2	374.6	375.1	375.2	0.53%
(3,2)*	734.8	733.6	732.8	732.4	728.7	729.8	730.0	0.33%
(0,4)	881.2	880.3	880.3	879.8	873.3	875.5	876.1	0.42%
(4,0)	938.0	937.2	937.2	936.7	930.8	933.1	933.6	0.33%
(4,1)*	1111.4	1111.0	1109.9	1109.7	1099.8	1102.5	1103.2	0.59%
(3,3)	1538.0	1538.0	1532.0	1532.0	1522.3	1525.0	1525.7	0.42%
(2,4)	1707.2	1705.4	1705.4	1705.0	1695.4	1699.5	1700.5	0.26%
(4,2)	1837.3	1826.0	1826.0	1821.6	1807.7	1811.8	1812.8	0.49%

a decreasing sequence, whereas the finite difference ones form an increasing sequence. Thus, when the relative gap is small (e.g., less than 1%), we can be confident that the true eigenvalue lies within this interval and is well approximated by the average of the two values.

Taking this approximation as the "true" eigenvalue, we compare our results with the published results of Chladni [8] and Ritz [25]. In Figure 4.4, the height of the marker indicates the eigenvalue found by either Chladni or Ritz, plotted against our computed values along the x-axis. We see that both men obtained exceptionally accurate results, considering Chladni relied on his ear for the frequencies and Ritz solved the eigenvalue problems without the help of a computer!

We further observe that Ritz tended to overestimate the eigenvalues (cf. the beginning of section 3.1), whereas Chladni tended to underestimate them. The overestimation by Ritz can be explained mathematically: since he is replacing a minimization problem in an infinite-dimensional function space by an approximate minimization in

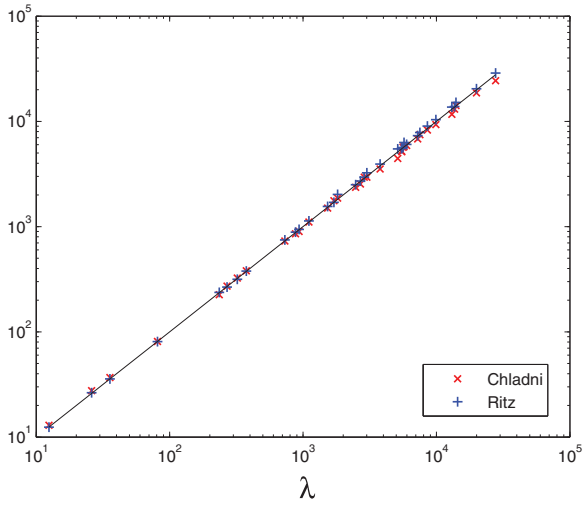

Fig. 4.4 *Eigenvalues found by Chladni and Ritz.*

a finite-dimensional subspace, the approximate minimum must be larger than the true minimum. Thus, his values are necessarily overestimations of the true values. The same reasoning also explains why the eigenvalues we obtained using the spectral method form a decreasing sequence: by increasing the number of basis functions, we are searching in an ever larger subspace, over which the minimum must become smaller. As for Chladni's underestimation, remember that his results come from observed frequencies produced with an experimental apparatus. Thus, we contend that the error stems from friction in the real physical system, since friction tend to lower the frequency of vibration when compared with the ideal (frictionless) system.

4.3. Suspension Bridges. If we want to calculate the eigenmodes of a thin plate that qualitatively resembles the shape of an oscillating bridge, different boundary conditions must be applied at the two ends of the bridge, since the bridge must be fixed and not allowed to move freely there. If we observe the video of the Tacoma bridge carefully, we see that the center span of the bridge is supported by girders located at the two towers. This means there is no vertical displacement at the towers (i.e., at the two ends of the center span), so we must impose the boundary condition

$$u = 0, \qquad x = \pm L, \quad y \in (-H, H). \tag{4.1}$$

Note that this is an *essential boundary condition*, meaning that it must be included as a constraint in the min-max problem (2.22), i.e. all the functions in the space U must satisfy it. This is because the admissible deformations $\varepsilon v(x, y)$ in (2.3) must also satisfy $v = 0$ at the two ends, so that deformations that change the position of the bridge at the anchor points are disallowed. Thus, the constrained minima of the energy functional are different (with the value of the functional necessarily higher) than the unconstrained minima.

To derive the complete set of boundary conditions for the strong form, we refer

back to (2.17). Since $v = 0$ at $x = \pm L$, the term

$$\int_{\partial\Omega} \big[u_{xxx} + (2-\mu)u_{xyy}\big] v n_x \, ds$$

must vanish along $x = \pm L$. This means the edge conditions (2.19) must be replaced by

$$u = 0, \qquad u_{xx} + \mu u_{yy} = 0, \qquad x = \pm L, \quad y \in (-H, H),$$

or, using the fact that $u = 0$ implies $u_{yy} = 0$ along the edge,

$$u = u_{xx} = 0, \qquad x = \pm L, \quad y \in (-H, H). \tag{4.2}$$

Note that without the variational form, it would be difficult to know exactly which boundary condition to keep and which one to remove.

If we were to use Ritz's method to solve the bridge problem, we would need to use 1D eigenfunctions that staisfy (4.2) in the x-direction rather than (3.2), i.e., different integrals will need to be evaluated. On the other hand, the finite difference code can be adapted much more easily: all we need to do is to impose $u = u_{xx} = 0$ on two of the four boundaries:

```
A(bl,:) = 0; A(bl,bl) = speye(length(bl));  % left boundary points
A(br,:) = 0; A(br,br) = speye(length(br));  % right boundary points
for i=gl',  %left ghost points
    A(i,:) = 0; A(i,[i+1,i,i+2]) = [2, -1, -1];
end;
for i=gr',  %right ghost points
    A(i,:) = 0; A(i,[i-1,i,i-2]) = [2, -1, -1];
end;
```

We can now eliminate the boundary points (in addition to the ghost points) by taking a Schur complement. We run the modified code to obtain the two eigenmodes that qualitatively approximate the vibrations in our two bridge examples. The plots are shown in Figure 4.5, along with photos of the two bridges extracted from the videos.

5. Related Problems and Further Reading. PDE eigenvalue problems are a fascinating subject, and we have only touched on a few aspects in this paper. In connection with nodal lines and Chladni figures, there is the famous nodal line theorem: for the simple case of a vibrating string, it is well known that it is divided into exactly k nodal intervals by the zeros of its k-th eigenfunction. For a two-dimensional membrane modeled by the Laplace equation, Courant's nodal line theorem states that k is an upper bound for the number of nodal domains of the k-th eigenfunction, see for example [22] and [2]. It would be interesting to see whether this conclusion also holds for the elastic plate, which is modeled by the biharmonic equation. One can also go a step further and ask if it is possible to find the potential from given nodal lines, also known as the inverse nodal problem [13]. A closely related inverse problem for the Laplace operator is whether one can hear the shape of a drum, see the famous article by Mark Kac [16]. Ritz did in fact solve an inverse problem himself: to match his calculations with Chladni's experimental data, he needed the value of the material density. However, Chladni had not stated in his work if the plates he used were made of glass or metal, or both. So in order to determine this, Ritz compared his pitch

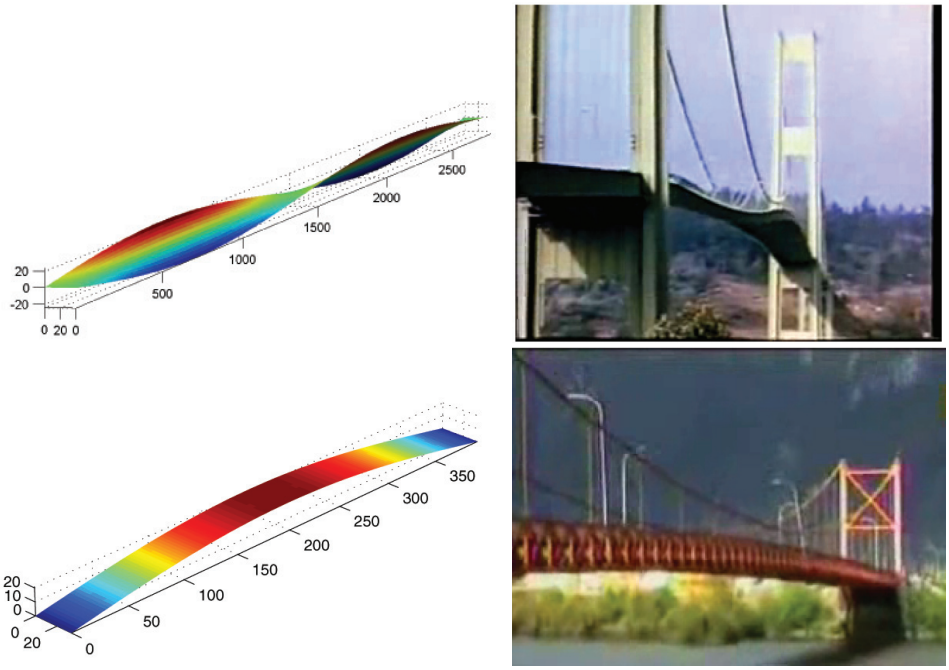

Fig. 4.5 *Top: A comparison of an eigenmode of a thin plate to the shape of the Tacoma Bridge shortly before its collapse. Bottom: A comparison of an eigenmode of a thin plate with the shape of the bridge oscillation excited by the earthquake in Puerto Aysén, Chile.*

calculations to the pitch values in the tables of Chladni, and found that for agreement, the density must have been that of glass[5].

Lastly, we would like to note that we have only considered one particular spectral method, and one finite difference method, for the biharmonic operator. There are many other discrete formulations; in particular we would like to mention the finite element methods presented in [14], and the finite difference methods proposed by [5, 18, 23, 24], see also the recent paper [3].

Appendix. MATLAB Code for Chladni Figures.

```
n = 100;      % Number of points per direction (includes ghost points)
mu = 0.225;   % Material constant
h = 2/(n-3);  % Distance between grid points
M = 90;       % Number of eigenvalues desired

% Set up grid
G = numgrid('S',n+2); D = delsq(G);

% Define boundary and ghost points
bl = G(3:n,3); br = G(3:n,n);   bt = G(3,3:n)'; bb = G(n,3:n)';
gl = G(3:n,2); gr = G(3:n,n+1); gt = G(2,3:n)'; gb = G(n+1,3:n)';
```

[5] ... im allgemeinen jedoch zeigt die Übereinstimmung mit unserer für Glas ausgeführten Rechnung, dass er Glasplatten benutzt hat.

```
% Initialize N and L to the discrete Laplacian
L = D; N = D;

% Correct outer Laplacian N for boundary conditions
N(bl,bl) = N(bl,bl)/2; N(br,br) = N(br,br)/2;
N(bt,bt) = N(bt,bt)/2; N(bb,bb) = N(bb,bb)/2;

% Trick: Modify the stencil in L at the ghost points to approximate
% ddu/dndt, which gives the correct boundary conditions
L([gl;gr;gt;gb],:) = 0;
for i=gl(1:end-1)',  %left
    L([i,i+1],[i,i+1,i+2*n,i+2*n+1]) = ...
    L([i,i+1],[i,i+1,i+2*n,i+2*n+1]) + (mu-1)/2*[1,-1,-1,1;-1,1,1,-1];
end;

for i=gr(1:end-1)',  %right
    L([i,i+1],[i,i+1,i-2*n,i-2*n+1]) = ...
    L([i,i+1],[i,i+1,i-2*n,i-2*n+1]) + (mu-1)/2*[1,-1,-1,1;-1,1,1,-1];
end;

for i=gt(1:end-1)',  %top
    L([i,i+n],[i+n,i,i+n+2,i+2]) = ...
    L([i,i+n],[i+n,i,i+n+2,i+2]) - (mu-1)/2*[1,-1,-1,1;-1,1,1,-1];
end;

for i=gb(1:end-1)',  %bottom
    L([i,i+n],[i+n,i,i+n-2,i-2]) = ...
    L([i,i+n],[i+n,i,i+n-2,i-2]) - (mu-1)/2*[1,-1,-1,1;-1,1,1,-1];
end;

% Compose N and L to get 4th order operator
A = N*L;

% Use boundary conditions to eliminate ghost points
A([gl; gr; gt; gb],:) = 0;
for i=gl',  %left
    A(i,[i+n,i,i+n-1,i+n+1,i+2*n]) = [2*(1+mu), -1, -mu, -mu, -1];
end;
for i=gr',  %right
    A(i,[i-n,i,i-n-1,i-n+1,i-2*n]) = [2*(1+mu), -1, -mu, -mu, -1];
end;
for i=gt',  %top
    A(i,[i+1,i,i+1+n,i+1-n,i+2]) = [2*(1+mu), -1, -mu, -mu, -1];
end;
for i=gb',  %bottom
    A(i,[i-1,i,i-1+n,i-1-n,i-2]) = [2*(1+mu), -1, -mu, -mu, -1];
end;

% Eliminate ghost points
phys = G(3:n,3:n); phys = phys(:); % put all physical nodes in a vector
ghost = [gl; gr; gt; gb];
A0 = A(phys,phys) - A(phys,ghost)/A(ghost,ghost)*A(ghost,phys);

% RHS: take into account half cells and quarter cells
```

```
B = speye(n^2);
B(bl,bl) = B(bl,bl)/2; B(br,br) = B(br,br)/2;
B(bt,bt) = B(bt,bt)/2; B(bb,bb) = B(bb,bb)/2;
B0 = B(phys,phys);

% Generalized eigenvalue problem
[V,Lambda] = eigs(A0/h^4,B0,M,'SM');
[y,p] = sort(diag(Lambda));
x=[-1:2/(n-3):1];

for i=4:M,  % plot Chladni figures
    contour(x,x,reshape(V(:,p(i)),n-2,n-2),[0 0],'k-');
    axis equal
end;
```

REFERENCES

[1] *NOVA Online: Super Bridge*. Available online from http://www.pbs.org/wgbh/nova/bridge/meetsusp.html, 2000.

[2] G. Alessandrini, *On Courant's nodal domain theorem*, Forum Math., 10 (1998), pp. 521–532.

[3] M. Ben-Artzi, I. Chorev, J.-P. Croisille, and D. Fishelov, *A compact difference scheme for the biharmonic equation in planar irregular domains*, SIAM J. Numer. Anal., 47 (2009), pp. 3087–3108.

[4] K. Y. Billah and R. H. Scanlan, *Resonance, Tacoma Narrows bridge failure, and undergraduate physics textbooks*, Amer. J. Phys., 59 (1991), pp. 118–124.

[5] J. H. Bramble, *A second-order finite difference analog of the first biharmonic boundary value problem*, Numer. Math., 9 (1966), pp. 236–249.

[6] I. G. Bubnov, *Structural Mechanics of Shipbuilding*, 1914 (in Russian).

[7] E. F. F. Chladni, *Die Akustik*, Leipzig, 1802. Available online from http://vlp.mpiwg-berlin.mpg.de/references?id=lit29494.

[8] E. F. F. Chladni, *Neue Beiträge zur Akustik*, in Entdeckungen über die Theorie des Klanges, Leipzig, 1821.

[9] B. G. Galerkin, *Rods and plates. Series occurring in various questions concerning the elastic equilibrium of rods and plates*, Engineers Bulletin (Vestnik Inzhenerov), 19 (1915), pp. 897–908 (in Russian).

[10] M. J. Gander and G. Wanner, *From Euler, Ritz, and Galerkin to modern computing*, SIAM Rev., 54 (2012), to appear.

[11] S. Germain, *Recherches sur la théorie des surfaces élastiques*, Mme. Veuve Courcier, Paris, 1821.

[12] S. Germain, *Remarques sur la nature, les bornes et l'étendue de la question des surfaces élastiques, et l'équation générale de ces surfaces*, Mme. Veuve Courcier, Paris, 1826.

[13] O. H. Hald and J. McLaughlin, *Inverse nodal problems: Finding the potential from nodal lines*, Mem. Amer. Math. Soc., 119 (1996).

[14] T. J. R. Hughes, *The Finite Element Method: Linear Static and Dynamic Finite Element Analysis*, Prentice-Hall, Englewood Cliffs, NJ, 1987.

[15] C. Johnson, *Numerical Solutions of Partial Differential Equations by the Finite Element Method*, Cambridge University Press, Cambridge, UK, 1987.

[16] M. Kac, *Can one hear the shape of a drum?*, Amer. Math. Monthly, 73 (1966), pp. 1–23.

[17] G. Kirchhoff, *Über das Gleichgewicht und die Bewegung einer elastischen Scheibe*, J. Reine Angew. Math., 40 (1850), pp. 51–88.

[18] J. R. Kuttler, *A finite-difference approximation for the eigenvalue of the clamped plate*, Numer. Math., 17 (1971), pp. 230–238.

[19] H. Lamb, *On the flexure of an elastic plate*, Proc. London Math. Soc., 21 (1889), pp. 70–91.

[20] A. C. Lazer and P. J. McKenna, *Large amplitude periodic oscillations in suspension bridges: some new connections with nonlinear analysis*, SIAM Rev., 32 (1990), pp. 537–578.

[21] P. J. McKenna, *Large torsional oscillations in suspension bridges revisited: Fixing an old approximation*, Amer. Math. Monthly, 106 (1999), pp. 1–18.

[22] A. Pleijel, *Remarks on Courant's nodal line theorem*, Comm. Pure Appl. Math., 9 (1956), pp. 543–550.

[23] V. G. Prikazchikov, *The finite difference eigenvalue problem for fourth-order elliptic operator*, U.S.S.R. Comput. Math. Math. Phys., 17 (1978), pp. 89–99.

[24] V. G. Prikazchikov and A. N. Khimich, *The eigenvalue difference problem for the fourth order elliptic operator with mixed boundary conditions*, U.S.S.R. Comput. Math. Math. Phys., 25 (1985), pp. 137–144.

[25] W. Ritz, *Theorie der Transversalschwingungen einer quadratischen Platte mit freien Rändern*, Ann. Physik, 18 (1909), pp. 737–807.

[26] H. Slogoff and B. Berner, *A simulation of the Tacoma Narrows bridge oscillations*, The Physics Teacher, 38 (2000), pp. 442–443.

[27] W. A. Strauss, *Partial Differential Equations: An Introduction*, John Wiley, New York, 1992.

[28] J. W. Strutt (Baron Rayleigh), *The Theory of Sound*, Vol. I, Macmillan, London, 1894. New edition, Dover, New York, 1945.

[29] S. S. P. Timoshenko, *Sur la stabilité des systèmes élastiques*, Annales des Ponts et Chaussées, 9 (1913), pp. 496–566. Translated from Russian by Jean Karpinski and Victor Héroufosse; originally published in Isvestija Kievskogo Politechnitscheskogo Instituta, Kiev, 1910.

[30] J. H. Wilkinson, *The Algebraic Eigenvalue Problem*, Oxford University Press, Oxford, 1965.